Research Article

ThanhTrung Trang*, ThanhLong Pham, Yueming Hu, Weiguang Li, and Shoujin Lin

Modelling and graphing the Wi-Fi wave field using the shape function

https://doi.org/10.1515/phys-2022-0196
received April 26, 2022; accepted July 27, 2022

Abstract: This article deals with modelling the Wi-Fi wave field, which is not visible to the naked eye, into a mathematical structure for assigning colours to observe the wave strength change compared to the source layout's location correlation of obstacles in the survey environment. The shape function is used as a tool in modelling combined with finite sample measurement data to determine the basic parameters of the shape function. These will allow the wave field to be modelled using two techniques: the theoretical shape function and the experimental shape function. The measuring tool used in the article is the Wi-Fi Analyzer App that runs on a smartphone. The colour-assigned representation of an invisible field such as a wave will help select the signal maximal or minimization positions most beneficial to the user. The proposal is easily applied in the wave field and other quantities such as temperature, light, and concentration with similar techniques.

Keywords: shape function, modelling, Wi-Fi wave field, graphical spectrum

*** Corresponding author: ThanhTrung Trang,** School of Automation Science and Engineering, South China University of Technology, Guangdong, China; R&D Technology Center, Zhongshan Mltor CNC Technology Co., Ltd, Guangdong, China,
e-mail: 202021002314@mail.scut.edu.cn
ThanhLong Pham: Division of Mechatronics, Faculty of Mechanical Engineering, Thai Nguyen University of Technology, Thai Nguyen, Vietnam, e-mail: Kalongkc@tnut.edu.vn
Yueming Hu: School of Automation Science and Engineering, South China University of Technology, Guangdong, China,
e-mail: auymhu@scut.edu.cn
Weiguang Li: School of Mechanical and Automotive Engineering, South China University of Technology, Guangdong, China,
e-mail: wguangli@scut.edu.cn
Shoujin Lin: General Manager's Office, Zhongshan Mltor CNC Technology Co., Ltd, Guangdong, China,
e-mail: harryLin@mltor.com

1 Introduction

Many physical fields exist around us but cannot be seen by the naked eye, exploiting these fields to maximize or minimize them needs to be based on understanding the spatial distribution as to how that is to observe them. Much research focused on showing the distribution of physical fields, such as Shimada *et al.* [1] studied the visualization of the spatial dispersion of optical fields in the gold nanoparticles' spacetime linear array structures using scanning near-field optical microscopy and electron microscopy. Le Kien *et al.* [2] studied the characterization of the guided normal field in parallelly coupled optical nanofibres. Research has shown the relationship between the spatial distributions of the field components of nanofibres and the electric field components. Sha *et al.* [3] used the corner transport upwind and constrained transport algorithm to study the digital interaction between the plane shock wave and the gas column in a magnetic field.

One of the popular ideas for exploiting the fields is to represent the field with mathematical modelling and assign a colour to the intensity variable to represent the field in a rainbow spectrum or digitizing graphically. Some recent studies are based on this idea. For example, Erturk *et al.* [4] used fractional calculus theory to study the movement of a beam on an internally bent nanowire. Then, Jajarmi *et al.* [5] used the classical Lagrangian method, establishing the Euler–Lagrange equations to study the complex displacement and charge of the condenser microdynamic system. Most recently, Baleanu *et al.* [6] used the structure of fractional derivatives and integrals to investigate the generalized fractional model of COVID-19, considering the effects of isolation and quarantine. Also, by using the generalized fractional model, Jajarmi *et al.* [7] researched the asymptotic behaviour of immunogen tumour dynamics.

Some physical area fields have specialized equipment that makes them visual. For example, the temperature field can use thermal imaging cameras to examine its distribution directly, but the cost of the equipment is

prohibitive. In addition, the approach using the interpolated function in combination with sensors to study physical fields such as temperature is also mentioned by many research studies. Oktavia *et al.* [8] used spatial interpolation in combination with five sensors to control temperature and humidity in data centre rooms. Wang *et al.* [9] used surface spline interpolation to investigate and control the temperature of integrated circuits. Bullo *et al.* [10] calculated the thermal field distribution of complex biological structures using the quadratic interpolation method. Long *et al.* [11] also studied the calculation of the thermal field distribution but used a shape function to interpolate.

Moreover, many other physical areas are not visible to the naked eye and require a solution to visualize them, so a method for this problem is issued [12]. For the Wi-Fi wave field, its intensity satisfies the continuity in space. Therefore, they can be interpolated by approximation and continuous functions, precisely the shape function of the form [13,14]. Many authors have interpolated quantities, such as wave fields, error, or material with positive results, as long as they satisfy the continuity condition and they are approximated with a polynomial function. Gilewski and Pelczynski [15] used shape functions to solve material orientation problems for a moderately thick plate of functionally graded materials. Liu and Chang [16] used a concept called the boundary shape function to calculate and automate the quadratic nonlinear boundary-value problem satisfying the constraints. Xia *et al.* [17] compared the study with the Lasserre algorithm and showed that the shape function derivative is more intuitive and can be programmed conveniently. Silva *et al.* [18] compared the use of finite-element mesh and shape functions to determine the degrees of freedom of the mesh at the data point coordinates. The research results have shown that the interpolation using the element shape functions is more than correct. Hou and Shi [19] used a shape function that generalizes data-driven time-frequency analysis to describe the frequency modulation of an intra-wave. Research has also shown that it is an efficient and powerful adaptive time-frequency analysis method for intrawave frequency signals.

Because in the same environment or office using the same Wi-Fi transmitter, users in different locations catch signals with different strengths and weaknesses. Furthermore, it is often impossible to determine the exact location of the most robust signal to use other than signal testing. So, using a finite number of measurements with a simple device combined with shape function interpolation, which is a robust and efficient method to analyse digital waveform signals, as studies [18,19] have shown, displaying the Wi-Fi wave field graphically or numerically to help choose the most profitable, maximum, or minimum position signal for users is the driving force behind this study. With some data measured by the Wi-Fi Analyzer App on a smartphone, it is possible to determine the mathematical function that describes the Wi-Fi wave field in the survey space and draw the corresponding distribution. This approach allows for selecting suitable areas for the requirements of using space in parallel with using WiFi. This idea applies to the Wi-Fi wave field and can also be applied to any field quantity that satisfies the continuum and cannot be observed with the naked eye. The article's success opens up a direction for modelling field-type quantities with a lower cost of time and equipment than using specialized equipment, sometimes without specialized observation equipment. This is the most effective way to fix this problem up to now, which is the main contribution of the research team.

The article is organized as follows. Section 2 introduces the concept of the shape function, the theoretical shape function, and the form of the experimental shape function. Then, the coordinate survey space, the device to measure the Wi-Fi signal using the Wi-Fi Analyzer App, the calculation method to simulate the Wi-Fi wave function in the form of the colour spectrum, and numerical graphs are presented in Section 3. Finally, we conclude in Section 4.

2 Theoretical shape function and experimental shape function form

2.1 Concept of a shape function

The shape function is commonly used in interpolation [13,14] and has many different forms suitable for different situations. For example, an interpolated space was considered, as shown in Figure 1.

In Figure 1, the intensity influence of scalar sources $\eta_1, \eta_2, \ldots, \eta_n$ on the survey point P_i is calculated according to the superposition principle described by the following equation:

$$\eta_{pi} = N_1^{(i)} \cdot \eta_1 + N_2^{(i)} \cdot \eta_2 + \cdots + N_n^{(i)} \cdot \eta_n, \tag{1}$$

where the coefficients $N_1, N_2, \ldots, N_n$ are the shape functions describing the influence of sources $\eta_1, \eta_2, \ldots, \eta_n$ on the survey point. The shape function of a key point will give a maximum influence value of one at that point and

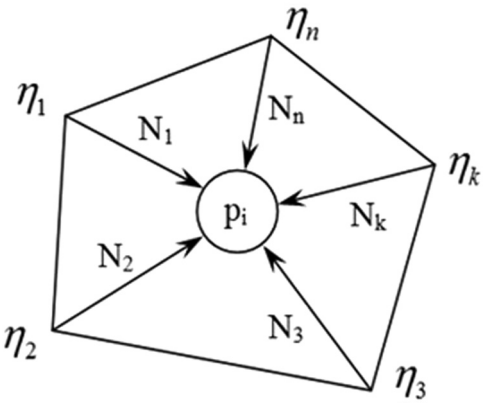

Figure 1: The influence of the key points of the survey point through the shape functions.

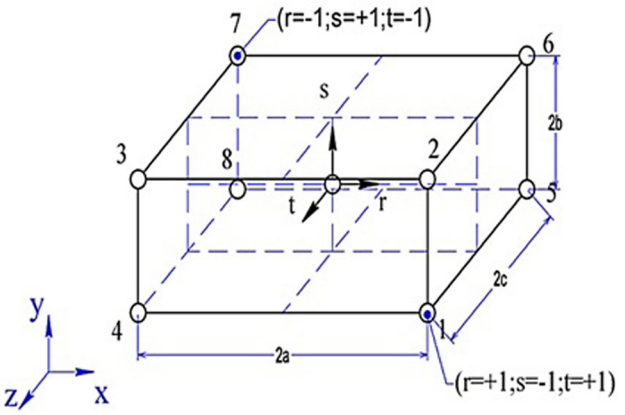

Figure 2: The key points and reference systems in the survey area.

decrease to zero at the remaining points, Eq. (1) describes the principle of superposition at the survey point. Either of the following two methods can determine the shape functions N_i.

2.2 Theoretical shape functions

By considering a survey area in a rectangular box, as shown in Figure 2, the theoretical shape function for the eight key points in Figure 2 is determined as follows:

$$\begin{aligned}
N_1 &= \frac{1}{8}(1+r)(1-s)(1+t),\\
N_2 &= \frac{1}{8}(1+r)(1+s)(1+t),\\
N_3 &= \frac{1}{8}(1-r)(1+s)(1+t),\\
N_4 &= \frac{1}{8}(1-r)(1-s)(1+t),\\
N_5 &= \frac{1}{8}(1+r)(1-s)(1-t),\\
N_6 &= \frac{1}{8}(1+r)(1+s)(1-t),\\
N_7 &= \frac{1}{8}(1-r)(1+s)(1-t),\\
N_8 &= \frac{1}{8}(1-r)(1-s)(1-t).
\end{aligned} \tag{2}$$

The reference system (r, s, t) is located at the centre of the box, so the formula for shifting the axis is written as follows:

$$r = \frac{x - x*}{a},\ s = \frac{y - y*}{b},\ t = \frac{z - z*}{c}, \tag{3}$$

in which a, b, c are determined according to Figure 2, the coordinates of the centre of gravity of the element under consideration is written as follows:

$$x^* = \frac{x_1 + x_4}{2},\ y^* = \frac{y_1 + y_2}{2},\ z^* = \frac{z_1 + z_3}{2}. \tag{4}$$

Thus, these values (r, s, t) vary in the range $[-1, 1]$, and as a result, the N_i values also belong to the $[-1, 1]$ interval after changing the variable.

2.3 Experimental shape functions

Like the theoretical shape functions, the N_i values in Eq. (1) can be the stationary value of the coordinate function $f_i(x, y, z)$, which is the function of the distances of the corresponding coordinates.

$$\begin{cases} f_1(x, y, z)_{pi} = N_1 \\ \quad\vdots \qquad\qquad i = 1 \div n. \\ f_n(x, y, z)_{pi} = N_n \end{cases} \tag{5}$$

The function $f_i(x, y, z)$ on the left side of Eq. (5) is the experimental shape function, and N_i is the stationary value of this function calculated for different survey points P_i. According to Figure 1, a point P_i is surveyed inside the field of n key points with known $(\eta_1, \eta_2 \dots \eta_n)$ error, including the error of the survey point η_{P_i}. Considering the components of the measured data at the survey point P_i including $\eta_{pi} = (d_x, d_y, d_z, \theta_x, \theta_y, \theta_z)^{(p_i)}$, this relationship can be expressed in terms of the values of the known key points as follows:

$$\begin{cases} \eta_1^{pi} = N_1 \cdot d_x^{(1)} + N_2 \cdot d_x^{(2)} + \dots + N_n \cdot d_x^{(n)} \\ \quad\vdots \\ \eta_n^{pi} = N_1 \cdot \theta_z^{(1)} + N_2 \cdot \theta_z^{(2)} + \dots + N_n \cdot \theta_z^{(n)}. \end{cases} \tag{6}$$

From here, the stationary value of experimental shape functions is determined for the point P_i.

$$\begin{bmatrix} N_1 \\ \vdots \\ N_n \end{bmatrix}_{pi} = \begin{bmatrix} d_x^{(1)} & \cdots & d_x^{(n)} \\ \cdots & \cdots & \cdots \\ \theta_z^{(1)} & \cdots & \theta_z^{(n)} \end{bmatrix}^{-1} \cdot \begin{bmatrix} d_x^{pi} \\ \cdots \\ \theta_z^{pi} \end{bmatrix}. \tag{7}$$

A unique set of stationary values according to equation (7) is not enough to determine a function of general form, it is necessary to continue investigating other points, such as examining points $P_1, P_2, \ldots, P_m$ to obtain:

$$\begin{bmatrix} N_1 \\ \vdots \\ N_n \end{bmatrix}_{p1}, \quad \begin{bmatrix} N_1 \\ \vdots \\ N_n \end{bmatrix}_{p2}, \ldots, \begin{bmatrix} N_1 \\ \vdots \\ N_n \end{bmatrix}_{pm}. \tag{8}$$

Thus, the regression law allows onto determine the experimental shape functions at the ith source as follows:

$$(N_{p1}^{(i)}, N_{p2}^{(i)}, \ldots, N_{pm}^{(i)}) \Rightarrow f_i(x, y, z). \tag{9}$$

3 Simulation and experiment

3.1 Space, frame of reference, and survey object

Figure 3 is a model of a room with the Wi-Fi transmitter placed outside, assuming that walls with different textures and distances from Wi-Fi transmitters will cause different effects on wave strength. The Wi-Fi wave strength at the eight corners of the room are measured, which are the eight points of the model: A', A, B', B, C', C, D', D, and a point at O' in the middle of the room. According to the diagram, dimensions include the following:

$$\begin{aligned} AD &= 2a = 4{,}800 \ (\text{mm}), \\ AA' &= 2b = 2{,}500 \ (\text{mm}), \\ AB &= 2c = 3{,}200 \ (\text{mm}). \end{aligned} \tag{10}$$

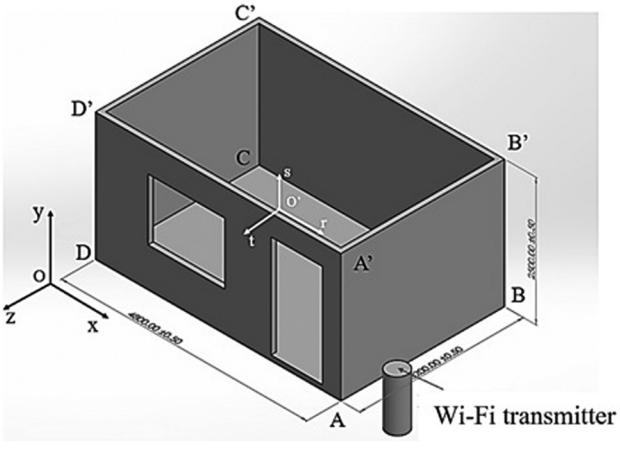

Figure 3: Spatial model of wave strength survey.

The coordinate system is placed at the centre of the room:

$$\begin{aligned} 2a &= 4{,}800 \Leftrightarrow a = 2{,}400 \ (\text{mm}), \\ 2b &= 2{,}500 \Leftrightarrow b = 1{,}250 \ (\text{mm}), \\ 2c &= 3{,}200 \Leftrightarrow c = 1{,}600 \ (\text{mm}). \end{aligned} \tag{11}$$

3.2 Measuring device

Wi-Fi Analyzer App (Android or IOS) is a popular application for mobile devices running Google or Apple's mobile operating systems, which includes the following features and characteristics:

- Optimize Wi-Fi for interference problems,
- Channel Analyzer for nearby APs,
- Real-time data and distance calculation,
- History of signal strength,
- Support 2.4 GHz/5 GHz,
- View Hidden Wi-Fi,
- Copy MAC address,
- Channel optimizer + more.

We see here the strength of the Wi-Fi signal in dBm (decibel milliwatts). These numbers are expressed as negative integers – the larger the negative integer, the stronger the signal. If the streaming video is needed, −67 dBm is the right pitch; for tasks that require less data like email, −70 dBm is sufficient intensity, and −30 dBm is the most robust signal strength. On the condition of wave strength, as shown in this article, this measuring device is acceptable for the accuracy of the measurement results.

Figure 4 shows the results of measurements at a location with various wireless transmitters that the app recorded. When measuring, it is necessary to place the machine at exact coordinates according to the global reference system as shown in Figure 3.

3.3 Calculation according to the theoretical shape function

The coordinates of the centroid $O'(r, s, t)$ are calculated as follows:

$$\begin{aligned} x^* &= \frac{4{,}800}{2} = 2{,}400, \\ y^* &= \frac{2{,}500}{2} = 1{,}250, \\ z^* &= \frac{-3{,}200}{2} = -1{,}600. \end{aligned} \tag{12}$$

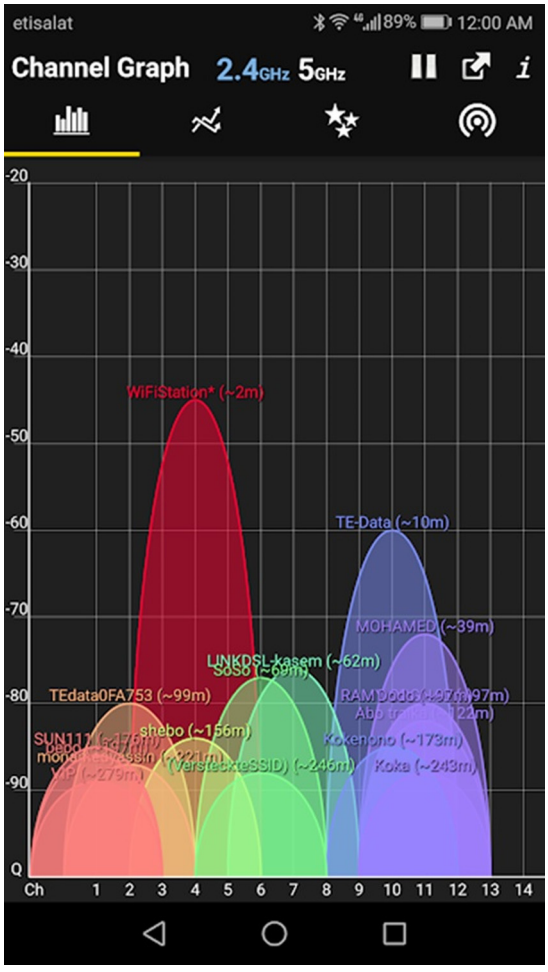

Figure 4: Wave strength at a survey measuring point using Wi-Fi analyzer software.

The variables are changed as follows:

$$r = \frac{x - 2{,}400}{2{,}400}, \quad s = \frac{y - 1{,}250}{1{,}250}, \quad t = \frac{z + 1{,}600}{1{,}600}. \tag{13}$$

The shape functions

$$\begin{aligned}
N_1 &= \frac{1}{8}\left(1 + \frac{x - 2{,}400}{2{,}400}\right)\left(1 - \frac{y - 1{,}250}{1{,}250}\right)\left(1 + \frac{z + 1{,}600}{1{,}600}\right),\\
N_2 &= \frac{1}{8}\left(1 + \frac{x - 2{,}400}{2{,}400}\right)\left(1 + \frac{y - 1{,}250}{1{,}250}\right)\left(1 + \frac{z + 1{,}600}{1{,}600}\right),\\
N_3 &= \frac{1}{8}\left(1 - \frac{x - 2{,}400}{2{,}400}\right)\left(1 + \frac{y - 1{,}250}{1{,}250}\right)\left(1 + \frac{z + 1{,}600}{1{,}600}\right),\\
N_4 &= \frac{1}{8}\left(1 - \frac{x - 2{,}400}{2{,}400}\right)\left(1 - \frac{y - 1{,}250}{1{,}250}\right)\left(1 + \frac{z + 1{,}600}{1{,}600}\right),\\
N_5 &= \frac{1}{8}\left(1 + \frac{x - 2{,}400}{2{,}400}\right)\left(1 - \frac{y - 1{,}250}{1{,}250}\right)\left(1 - \frac{z + 1{,}600}{1{,}600}\right),\\
N_6 &= \frac{1}{8}\left(1 + \frac{x - 2{,}400}{2{,}400}\right)\left(1 + \frac{y - 1{,}250}{1{,}250}\right)\left(1 - \frac{z + 1{,}600}{1{,}600}\right),\\
N_7 &= \frac{1}{8}\left(1 - \frac{x - 2{,}400}{2{,}400}\right)\left(1 + \frac{y - 1{,}250}{1{,}250}\right)\left(1 - \frac{z + 1{,}600}{1{,}600}\right),\\
N_8 &= \frac{1}{8}\left(1 - \frac{x - 2{,}400}{2{,}400}\right)\left(1 - \frac{y - 1{,}250}{1{,}250}\right)\left(1 - \frac{z + 1{,}600}{1{,}600}\right).
\end{aligned} \tag{14}$$

The interpolation function

$$\begin{aligned}
t = {} & N_1 \times t_1 + N_2 \times t_2 + N_3 \times t_3 + N_4 \times t_4 \\
& + N_5 \times t_5 + N_6 \times t_6 + N_7 \times t_7 + N_8 \times t_8,
\end{aligned} \tag{15}$$

with constraints

$$\begin{aligned}
0 \le x \le 4{,}800 \\
0 \le y \le 2{,}500 \\
-3{,}200 \le z \le 0
\end{aligned} \tag{16}$$

The survey results are obtained and calculated according to the theoretical shape function, as shown in Table 1. Note that the measurement results show a negative sign with the survey wave strength, so when assigning colours, the values have a smaller absolute value corresponding to the hot (red) colour spectrum. Larger absolute values correspond to the cool (blue) colour spectrum. These are because the colour spectrums used for the graphics must be continued in the rainbow spectrum to represent spatially varying wave intensities' transitions. In general, the graphics should represent

Table 1: Wi-Fi signal strength measurement results

Number of measurements	Point *A* (1)	Point *A′* (2)	Point *B* (5)	Point *B′* (6)	Point *C* (8)	Point *C′* (7)	Point *D* (4)	Point *D′* (3)
1	−38	−45	−49	−45	−79	−65	−63	−68
2	−39	−47	−52	−47	−77	−67	−66	−66
3	−39	−46	−53	−46	−77	−64	−65	−67
4	−40	−47	−55	−50	−81	−68	−69	−67
5	−42	−49	−57	−51	−80	−70	−68	−69
6	−41	−45	−51	−48	−75	−68	−67	−65
7	−43	−47	−53	−50	−78	−65	−64	−65
8	−41	−46	−51	−49	−77	−67	−65	−67
The average value	−40.37	−46.5	−52.62	−48.25	−78	−65.75	−65.87	−66.75

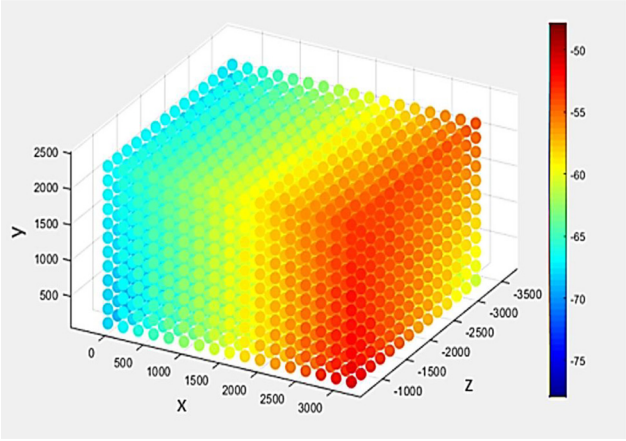

Figure 5: Graph of Wi-Fi wave strength in the room, according to the colour spectrum of the first observation direction.

the relative and absolute values of the wave strength at that point compared to the surrounding points.

Behind the wall where the Wi-Fi transmitter is placed with the most robust wave strength, in front of the wall, on the far side is the area with the slightest wave intensity (Figure 5). The fact that one of the two vertical walls has two doors like the room model also clearly affects the distribution of wave strength at the two longitudinal boundaries of the survey space. In particular, the side of the wall with the door opening Wi-Fi signal strength is stronger than the side without the door (Figure 6), showing that obstacles such as walls significantly affect the wave propagation and the propagation distance also affects the wave strength.

According to the second observation direction, the wave is most substantial in the wall corner near the Wi-Fi transmitter, adjacent to the room's door. The worst wave area is the wall intersection opposite to the transmitter on the far side and the vertical wall with no doors, which is the model's most distant and most hidden angle. The simulation results are entirely consistent with the retest results with the actual measuring device.

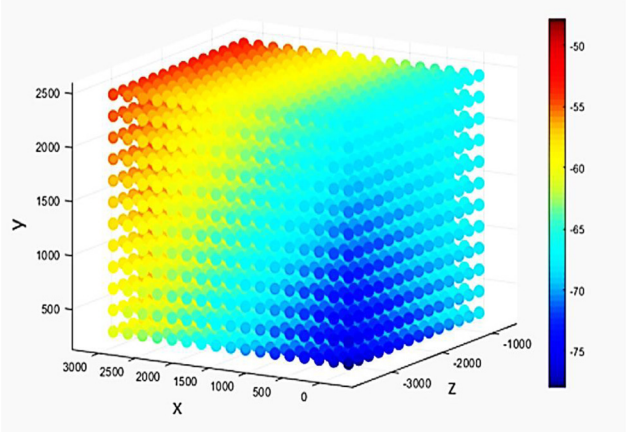

Figure 6: Graph of Wi-Fi wave strength in the room, according to the colour spectrum of the second observation direction.

4 Conclusion

Determining which location has the most substantial Wi-Fi waves to use in an area; how to arrange Wi-Fi transmitters to ensure that the entire area has the most robust wave strength and the lowest prices are the issues that users and Wi-Fi network design engineers are interested in. Unfortunately, there is no specialized device to display Wi-Fi wave images for an area, such as a thermal imaging camera to display the temperature field. Moreover, measurement, testing, or arranging sensors to locate the strongest or weakest Wi-Fi waves is very time-consuming and labour-intensive, requiring many measurements or many sensors to be arranged to obatin accurate data. Spatial shape function interpolation has been identified as an ideal solution for predicting Wi-Fi wave field data, a field data type with spatial continuity. By using the Wi-Fi Analyzer App, a simple application that runs on smartphones and has high reliability, to measure the value of Wi-Fi waves at specified points in the survey space. Using spatial shape function interpolation after calculating the display of all Wi-Fi wave images in the survey area has been performed.

Figures 5 and 6 show the results consistent with the actual distribution when the WiFi Analyzer App is re-tested. Thus, as long as the interpolated quantity is continuous and has suitable measuring equipment, it is possible to represent the magnitude distribution of any physical field graphically. Moreover, this technique is suitable for solving the problem in both directions, that is to find the wave intensity distribution and vice versa to find the wave strength to find the most satisfactory coordinate domain. The interpolation results are similar to Figures 5 and 6 in layout in determining experimental shape functions. However, the wave field has higher precision than the theoretical shape function due to many sample measurements.

The research team will continue to deepen the research and practical application of the proposed method by helping engineers design networks, especially in public places with high urbanization rates and high user demand for free Wi-Fi waves is very large. The problem is calculating

the location and the smallest number of Wi-Fi transmitters so that the area has the highest number of points to catch the most substantial Wi-Fi waves. In addition, as mentioned in Section 1, this technique can also be applied to solve problems related to temperature fields, such as calculating the number of points of heat generation needed to warm cattle on a farm in winter or the minimum number of heat points for a sanitary ware ceramic kiln with the requirement that all surfaces of the product be heated evenly to a temperature of 1,250° C. These are the topics that the research team will continue to develop in the future.

Funding information: The authors would like to acknowledge the Postdoctoral Science Foundation of China (Grant No. 2021M703780).

Author contributions: All authors have accepted responsibility for the entire content of this manuscript and approved its submission.

Conflict of interest: The authors state no conflict of interest.

Data availability statement: All data generated or analysed during this study are included in this published article.

References

[1] Shimada T, Imura K, Okamoto H, Kitajima M. Spatial distribution of enhanced optical fields in one-dimensional linear arrays of gold nanoparticles studied by scanning near-field optical microscopy. Phys Chem Chem Phys. 2013;15:4265–9.
[2] Le Kien P, Ruks L, Chormaic SN, Busch T. Spatial distributions of the fields in guided normal modes of two coupled parallel optical nanofibres. New J Phys. 2021;23:043006.
[3] Sha S, Huan-Hao Z, Zhi-Hua C, Chun Z, Wei-Tao W, Qi-Chen S. Mechanism of longitudinal magnetic field suppressed Richtmyer-Meshkov instability. Acta Physica Sinica 2020;69(18):184701.
[4] Erturk VS, Godwe E, Baleanu D, Kumar P, Asad J, Jajarmi A. Novel fractional-order Lagrangian to describe motion of beam on nanowire. Acta Phys Polonica A. 2021;140(3):265–72.
[5] Jajarmi A, Baleanu D, Zarghami Vahid K, Mohammadi Pirouz H, Asad JH. A new and general fractional Lagrangian approach: a capacitor microphone case study. Results Phys. 2021;31:104950.
[6] Baleanu D, Hassan Abadi M, Jajarmi A, Zarghami Vahid K, Nieto JJ. A new comparative study on the general fractional model of COVID-19 with isolation and quarantine effects. Alexandria Eng J. 2022;61(6):4779–91.
[7] Jajarmi A, Baleanu D, Zarghami Vahid K, Mobayen S. A general fractional formulation and tracking control for immunogenic tumour dynamics. Math Meth Appl Sci. 2022:45(2):667–80.
[8] Oktavia E, Widyawan W, Mustika IW. Inverse distance weighting and kriging spatial interpolation for data centre thermal monitoring. In: Proceedings of the First International Conference on Information Technology, Information Systems and Electrical Engineering, ICITISEE. 2016. p. 69–74.
[9] Wang R-L, Li X, Liu W-J, Liu T, Rong M-T, Zhou L. Surface spline interpolation method for thermal reconstruction with limited sensor data of non-uniform placements. J Shanghai Jiaotong Univ. 2014;19(1):65–71.
[10] Bullo M, D'Ambrosio V, Dughiero F, Guarnieri M. Coupled electrical and thermal transient conduction problems with a quadratic interpolation cell method approach. IEEE Trans Magn. 2006;42(4):1003–6.
[11] Long PT, Lê TT, Thang NH. Determining the parameter area at the request of a physical field based on shape function technique. In: International Conference on Engineering Research and Applications. 2018. p. 270–7.
[12] Liu G, Xiong J, Cao Y, Hou R, Zhi L, Xia Z, et al. Visualization of ultrasonic wavefield by stroboscopic polarization selective imaging. Optics Express. 2020;28(18):27096–106.
[13] Zienkiewicz OC, Taylor RL, Zhu JZ. The finite element method: its basis and fundamentals-chapter 6: shape functions. Derivatives and integration. Elsevier; 2013.
[14] Gao JB, Shih TM. Interpolation methods for the construction of the shape function space of nonconforming finite elements. Comput Methods Appl Mech Eng. 1995;122(1–2):93–103.
[15] Gilewski W, Pełczyński J. Material-oriented shape functions for FGM plate finite element formulation. Materials 2020;13(3):803.
[16] Liu C-S, Chang C-W. Boundary shape function method for nonlinear BVP, automatically satisfying prescribed multipoint boundary conditions. Boundary Value Problems. 2020;2020(139):1–22.
[17] Xia XZ, Jiang Q, and Zhang Q. Calculation of the derivative of interpolation shape function for three-dimensional natural element method. J Chin Inst Eng. 2016;39(3):363–71.
[18] Silva GHC, LeRiche R, Molimard J, Vautrin A. Exact and efficient interpolation using finite elements shape functions. European J Comput Mech. 2009;18(3–4):307–31.
[19] Hou TY, Shi Z. Extracting a shape function for a signal with intra-wave frequency modulation. Philosoph Trans R Soc A Math Phys Eng Sci. 2016;374(2065):20150194.